

Elliptic flow of thermal photons in heavy-ion collisions at Relativistic Heavy Ion Collider and Large Hadron Collider

H. Holopainen,^{*} S. S. Räsänen,[†] and K. J. Eskola[‡]

Department of Physics, P.O.Box 35, FI-40014 University of Jyväskylä, Finland and Helsinki Institute of Physics, P.O.Box 64, FI-00014 University of Helsinki, Finland

We calculate the thermal photon transverse momentum spectra and elliptic flow in $\sqrt{s_{NN}} = 200$ GeV Au+Au collisions at RHIC and in $\sqrt{s_{NN}} = 2.76$ TeV Pb+Pb collisions at the LHC, using an ideal-hydrodynamical framework which is constrained by the measured hadron spectra at RHIC and LHC. The sensitivity of the results to the QCD-matter equation of state and to the photon emission rates is studied, and the photon v_2 is discussed in the light of the photonic p_T spectrum measured by the PHENIX Collaboration. In particular, we make a prediction for the thermal photon p_T spectra and elliptic flow for the current LHC Pb+Pb collisions.

PACS numbers: 12.38.Mh, 25.75.Cj, 25.75.Ld

I. INTRODUCTION

Experimental data at the Relativistic Heavy Ion Collider (RHIC) and now also at the Large Hadron Collider (LHC) have shown compelling evidence of strongly interacting QCD-medium production in ultra-relativistic heavy-ion collisions. The measured transverse energies, transverse momentum (p_T) spectra and, in particular, the significant azimuthal anisotropy (elliptic flow) of final-state hadrons suggest together that partonic QCD matter, quark-gluon plasma (QGP), is formed in these collisions.

In the collision of two nuclei, the azimuthally anisotropic overlap region sets preferred directions for the transverse flow. In hydrodynamical models, pressure gradients turn the spatial anisotropy of the produced hot matter into a flow anisotropy, which is transmitted into the momentum distributions of measurable final-state hadrons at the decoupling of the system. However, the hadronic measurement reflects the flow (and temperature) conditions only in the freeze-out region where the hadronic interactions cease.

In comparison with partons, photons interact only very weakly with the QCD matter and thus a photon emitted from the medium most likely escapes from the system without interacting. This is seen also in the measurements where photons do not show a similar suppression as hadrons when we move from proton+proton (p+p) to nucleus+nucleus ($A + A$) collisions [1]. Since photons can escape from the medium without interacting, they carry information about the system at the time of their production.

Ultra-relativistic heavy-ion collisions are particularly interesting in regard with direct photon production, since relative to p+p collisions there are different types of nu-

clear effects at work as well as a number of important further sources for photons. In p+p (and also in p+A) collisions the direct photons are prompt photons originating from the primary hard interactions of partons, and fragmentation photons emitted by the primarily produced high- p_T partons [2]. In heavy-ion collisions (and also in p+A), both the prompt and fragmentation photons at high- p_T are subjected to nuclear effects in the parton distribution functions of the colliding nuclei (see e.g. [3, 4] for the quantification of these effects and their uncertainties). The fragmentation photon component is, however, expected to be suppressed due to the quenching of partonic jets in QCD matter in $A + A$ collisions. In addition to this, in $A + A$ collisions the jet(parton)-matter interactions, i.e. the jet-photon conversion [5, 6] and collision-induced photon emission from high-energy partons can produce photons which are important in the mid- p_T region [7–9]. Finally, the hot medium itself emits thermal photons, which are expected to be important in the few-GeV region and below, as discussed in the hydrodynamical studies of Refs. [7, 8, 10–13].

In heavy-ion collisions, it is very difficult to distinguish between the different direct photon sources. In addition, there is a huge decay-photon background to deal with. The elliptic flow of direct photons could, however, shed more light on the interplay of the various photon production sources which differ from each other as follows: At high- p_T (above ~ 5 GeV at RHIC), where prompt photons dominate [7], and where the fragmentation photons are more suppressed in the out-of-plane direction (perpendicular to the impact parameter), the photonic v_2 should be positive but very small [9]. The jet-medium interactions in turn increase the photon production most strongly in the in-plane direction (parallel to the impact parameter), thus causing a negative v_2 contribution at mid- p_T [9]. The thermal photon production is affected by the hydrodynamical transverse flow itself, so that photons in the in-plane direction get a stronger boost. As shown earlier in Refs. [14–16], this results in a positive elliptic flow for the thermal photons. Since the net contribution from other sources to photon v_2 is expected to be

^{*}Electronic address: hannu.l.holopainen@jyu.fi

[†]Electronic address: sami.s.rasanen@jyu.fi

[‡]Electronic address: kari.eskola@phys.jyu.fi

very small or even negative [9], a large (hadron-like) photon v_2 measured in the few- p_T region and below, should thus serve as a signature of thermal photon dominance. Since QCD matter is emitting photons throughout its entire evolution, measuring thermal photon p_T spectra and v_2 would thus give important further constraints for the dynamics and properties of QCD matter.

In this work we focus on computing the thermal photon p_T spectra and elliptic flow in $\sqrt{s_{NN}} = 200$ GeV Au+Au collisions at RHIC and in $\sqrt{s_{NN}} = 2.76$ TeV Pb+Pb collisions at the LHC, using an ideal-hydrodynamical framework which is constrained by the measured hadron spectra at RHIC and LHC. We study the sensitivity of the results to the QCD-matter equation of state (EoS) and to the photon emission rates. We discuss the photon v_2 in the light of the photonic p_T spectrum measured by the PHENIX Collaboration [17–19]. In particular, we make a prediction for the thermal photon p_T spectra and elliptic flow for the current LHC heavy-ion collisions. Previous predictions for the thermal photon p_T spectra in Pb+Pb collisions at the planned maximum cms-energy 5.5 TeV of the LHC can be found in [20, 21].

II. THEORETICAL FRAMEWORK

A. Centrality classes

Centrality classes for $A + A$ collisions studied here are calculated using the optical Glauber model. For nuclear densities we use spherically symmetric Woods-Saxon profiles with the thickness parameter $d = 0.54$ fm and radii $R_{Au} = 6.37$ fm and $R_{Pb} = 6.49$ fm. The total cross section for $A + A$ collisions is calculated from

$$\sigma_{\text{tot}}^{AA} = \int d^2\mathbf{b} \frac{d\sigma_{\text{tot}}}{d^2\mathbf{b}} = \int d^2\mathbf{b} \left(1 - e^{-T_{AA}(\mathbf{b})\sigma_{NN}^{\text{in}}}\right), \quad (1)$$

where T_{AA} is the standard nuclear overlap function and σ_{NN}^{in} is the inelastic nucleon-nucleon cross section. We take $\sigma_{NN}^{\text{in}} = 42(64)$ mb for $\sqrt{s_{NN}} = 200$ (2760) GeV.

The centrality classes are defined with impact parameter ranges $[b_i, b_{i+1}]$ so that for the centrality class of c_i we have

$$c_i = \frac{1}{\sigma_{\text{tot}}^{AA}} \int_{b_i}^{b_{i+1}} d^2\mathbf{b} \left(1 - e^{-T_{AA}(\mathbf{b})\sigma_{NN}^{\text{in}}}\right). \quad (2)$$

The average impact parameter for each centrality class is calculated using the distribution $d\sigma/d^2\mathbf{b}$ as a weight. The average number of participants is calculated similarly. The obtained centrality classes, impact parameter ranges, average impact parameters and number of participants are listed in Table I.

B. Initial states for hydrodynamical evolution

For RHIC we use the EKRT saturation model [22] to fix the initial entropy in most central collisions. As

shown in [23, 24] we can get a good description of the pion spectra and the elliptic flow with this pQCD + saturation + hydrodynamics approach. For Au+Au collisions at $\sqrt{s_{NN}} = 200$ GeV the model gives an initial time $\tau_0 = 0.17$ fm. For the $\sqrt{s_{NN}} = 2.76$ TeV Pb+Pb collisions at the LHC, we fix the initial entropy so that we reproduce the measured multiplicity [25]. The initial time $\tau_0 = 0.12$ fm is based on the EKRT-motivated fit done in Ref. [26].

To fix the initial transverse density profile in $\sqrt{s_{NN}} = 200$ GeV Au+Au collisions, we do the following: In Fig. 1 we show, from Ref. [27], the measured charged-particle multiplicity (divided by the number of participant pairs) as a function of the number of participants calculated from the optical Glauber model¹. Choosing the initial transverse density according to the binary-collision-scaled energy or entropy density (eBC, sBC), or wounded-nucleon-scaled energy or entropy density (eWN, sWN) as introduced in Ref. [28], we compute the charged-particle multiplicity in the centrality classes obtained above. The initial entropy at $b = 0$ in these four cases is kept fixed. We see that the sWN profile fits the measured centrality dependence quite well. We will therefore choose the sWN profile at RHIC and, for simplicity, use the same profile also for the LHC Pb+Pb collisions.

C. Hydrodynamics and freeze-out

To describe the spacetime evolution of the produced QCD matter, we solve the ideal-hydrodynamic equations

$$\partial_\mu T^{\mu\nu} = 0, \quad (3)$$

	centrality %	b range [fm]	$\langle b \rangle$ [fm]	N_{part}
	0-5	0.00-3.35	2.24	346
	5-10	3.35-4.74	4.08	289
	10-15	4.74-5.81	5.30	242
	15-20	5.81-6.71	6.27	202
	20-30	6.71-8.21	7.49	153
RHIC	30-40	8.21-9.49	8.87	102
	40-50	9.49-10.6	10.1	64.4
	50-60	10.6-11.6	11.1	37.5
	0-20	0.00-6.71	4.47	267
	20-40	6.71-9.49	8.18	128
	0-5	0.00-3.53	2.35	375
LHC	0-20	0.00-7.05	4.70	294
	20-40	7.05-9.98	8.60	141

TABLE I: Various centrality classes for Au+Au collisions at $\sqrt{s_{NN}} = 200$ GeV and for Pb+Pb collisions at $\sqrt{s_{NN}} = 2.76$ TeV, obtained via the optical Glauber model.

¹ Note that usually the number of participants quoted by the experiments here is from the MC Glauber model.

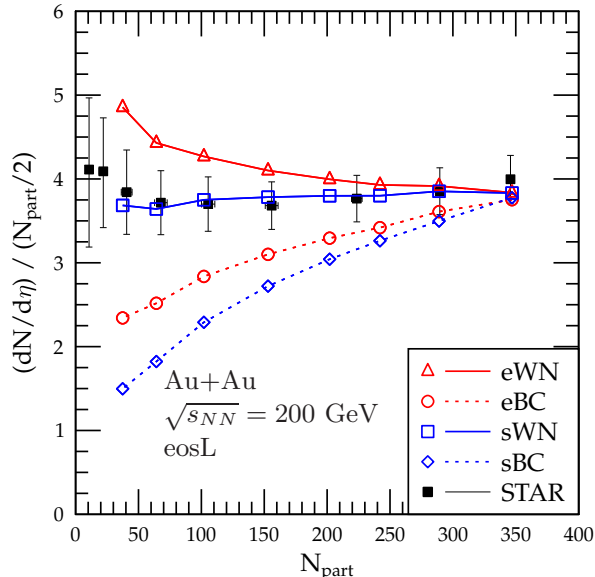


FIG. 1: (Color online) Number of charged hadrons at midrapidity in $\sqrt{s_{NN}} = 200$ GeV Au+Au collisions scaled by the number of the participant pairs calculated from the optical Glauber model. The data are from the STAR Collaboration [27].

where $T^{\mu\nu} = (\epsilon + P)u^\mu u^\nu - Pg^{\mu\nu}$ is the energy-momentum tensor, u^μ is the fluid four-velocity, ϵ is the energy density and P is the pressure. As we are interested in particle and photon production at midrapidity, we may assume that net-baryon density is negligible. Since the particle spectra are approximately flat at midrapidity, we can simplify our hydrodynamical equations by assuming longitudinal boost-invariance. We use the SHASTA algorithm [29, 30] to solve this (2+1)-dimensional numerical problem.

To close the hydrodynamic equations we need an Equation of state (EoS), $P = P(\epsilon)$. In this paper we study the sensitivity of thermal photon production to the EoS, by focusing on two different cases. The first case, called here "eosQ", corresponds to the Bag model EoS with a first order phase transition [31]. In eosQ, the high-temperature phase with the Bag constant is an ideal gas of three flavors of massless quarks and gluons, while the low-temperature phase is an ideal gas of all hadronic states with $m < 2$ GeV. These two phases are connected with a mixed phase, and the Bag constant is chosen so that the critical temperature is $T_c = 165$ MeV. The second EoS case, which we call "eosL", is adopted from Ref. [32]. This EoS is quite similar to the recently constructed lattice EoS "s95-p" [33], and as discussed in [33], the hadron spectra and elliptic flow are in practice insensitive to the differences between eosL and s95-p.

Since the lattice data suggests that the phase transition

from the QGP to hadron gas (HG) is not of first order, one may consider the eosQ case somewhat unrealistic. However, the computation of thermal photon production in the phase-transition region requires well-defined QGP and hadron-gas fractions, which are available only in the eosQ case. With eosL, in the absence of such phase fractions, there are additional uncertainties in the thermal photon calculation related to the QGP and HG emission rates.

Thermal transverse momentum (p_T) spectra of hadrons are obtained using the Cooper-Frye method [34] where particle emission from a freeze-out hypersurface σ is calculated with

$$\frac{dN^f}{d^2p_T dy} = \int_{\sigma} f(x, p) p^\mu d\sigma_\mu, \quad (4)$$

where $f(x, p)$ is the momentum distribution function of a specific hadron type. We assume the system to decouple at a single constant temperature T_{dec} , which is fixed so that we get a good agreement with the measured p_T spectra of pions at RHIC. With eosQ, we have $T_{\text{dec}} = 140$ MeV, and 160 MeV with eosL.

After the thermal emission of particles from the freeze-out surface is calculated, we take into account the strong and electromagnetic 2- and 3-body decays. This treatment is essential since most of the stable particles in our case come from the decays of heavy resonances.

The p_T spectra of hadrons can be written as a Fourier series,

$$\frac{dN}{d^2p_T dy} = \frac{1}{\pi} \frac{dN}{dp_T^2 dy} \left(1 + \sum_{n=1}^{\infty} 2v_n \cos(n\phi) \right), \quad (5)$$

where ϕ is the hadron momentum's azimuthal angle with respect to the reaction plane defined by the impact parameter. Elliptic flow, v_2 , is the second coefficient in this series and it can be computed from

$$v_2(p_T) = \frac{\int d\phi \cos(2\phi) \frac{dN(b)}{dp_T^2 d\phi dy}}{\int d\phi \frac{dN(b)}{dp_T^2 d\phi dy}}. \quad (6)$$

Correspondingly, the p_T -integrated v_2 becomes

$$v_2 = \frac{\int d\phi \cos(2\phi) \frac{dN(b)}{d\phi dy}}{\int d\phi \frac{dN(b)}{d\phi dy}}. \quad (7)$$

D. Thermal photons emission from the hydrodynamical medium

The p_T spectra of thermal photons can be calculated from

$$\frac{dN^\gamma}{d^2p_T dy} = \int d^4x \Gamma(E^*(x), T(x)), \quad (8)$$

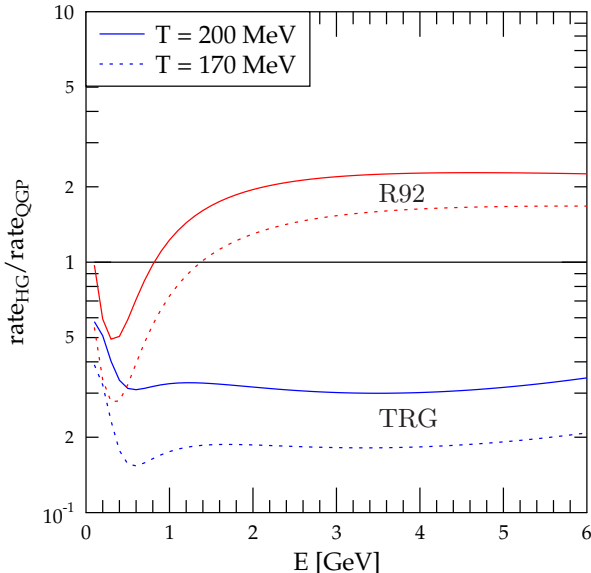


FIG. 2: (Color online) The HG-to-QGP ratio of the photon emission rates as a function of the photon energy at two different temperatures. Two different HG-rates, R92 [38–40] and TRG [41], are compared.

where $\Gamma(E^*, T)$ is the Lorentz invariant thermal photon emission rate, d^4x is the volume element and $E^*(x) = p^\mu u_\mu(x)$ is the photon energy in the fluid’s local rest frame. For the QGP, we use the emission rate from Refs. [35, 36] with $N_f = 3$ and a running strong coupling constant [37] $\alpha_s = \beta / \ln(8T/\Lambda)$, with $\beta = 6\pi / (33 - 2N_f)$ and $\Lambda = 200$ MeV. For the hadron gas, we use two different emission rates: (i) Those calculated in [38, 39] and parametrized in [39, 40], which we call ”R92”. These rates were used in the previously published LHC predictions [20]. (ii) The more recent ones from Ref. [41] which account also for the finite size of hadrons through form factors. We call these rates ”TRG”.

With eosL, which smoothly goes from the QGP to the HG phase without specifying their volume fractions, one needs to choose how to switch from the QGP to HG photon emission rates. For simplicity, we choose to do this at a constant temperature T_s but we vary T_s between 170 and 200 MeV. We label these two cases as ”eosL170” and ”eosL200”.

To illustrate the differences between the R92 and TRG emission rates which will be important for the photonic v_2 results presented in Sec. III ahead, we plot in Fig. 2 the ratio of the photon emission rates in the HG and QGP at two different fixed temperatures. We see that (since both HG rates have been divided by the same QGP rate) the difference between R92 and TRG is about a factor six at large energies. Furthermore, the TRG rates are always well below the QGP rates, while this is not the

case for the R92 rates.

Elliptic flow for the thermal photons is calculated as in Eq. (6). Since the thermal photons cannot be distinguished from other direct photons, the elliptic flow from thermal photons alone cannot be measured. In what follows, we assume that the net contribution to the photonic v_2 from the other direct photon sources remains small, especially since the fragmentation photons with a positive v_2 should partially cancel the negative v_2 of the photons arising from parton-medium interactions [9].

If other components are emitted isotropically we can roughly estimate how much they ”wash away” the elliptic flow coming from thermal photons. The total elliptic flow is then

$$v_2 = \left(\int d\phi \cos(2\phi) \frac{dN^{\text{th}}}{dp_T^2 d\phi dy} \right) \left(\int d\phi \frac{dN^{\text{all}}}{dp_T^2 d\phi dy} \right)^{-1} \quad (9)$$

$$= v_2^{\text{th}} \left(\frac{dN^{\text{th}}}{dp_T^2 dy} \right) \left(\frac{dN^{\text{all}}}{dp_T^2 dy} \right)^{-1},$$

where $dN^{\text{all}}/dp_T^2 dy$ corresponds to the measured p_T spectrum of direct photons and v_2^{th} is the v_2 of thermal photons alone.

III. RESULTS FOR RHIC

A. Hadron spectra and elliptic flow

First we show the hadronic observables to demonstrate that our hydrodynamical description of the bulk QCD-medium is reasonable. Figure 3 shows the transverse momentum spectra of positively charged pions in different centrality classes in $\sqrt{s_{NN}} = 200$ GeV Au+Au collisions at RHIC. As we can see, we have a good fit to the pion spectra below $p_T \approx 2$ GeV for a very wide range of centralities. The integrated elliptic flow of charged hadrons from Eq. (7) is plotted in Fig. 4 together with the data obtained by the STAR Collaboration [43] using the 4-particle cumulant and LYZ methods which should best reflect the elliptic flow relative to the reaction plane defined by the impact parameter. We have a fairly good description of the data also here, although the centrality dependence of the computed v_2 is not fully reproduced. We expect, however, that fine-tuning the initial density profile, invoking the Monte Carlo Glauber model and possibly also event-by-event hydrodynamics (see e.g. Ref. [44]) as well as including viscous effects (see e.g. Ref. [45]) will improve the agreement. These improvements are, however, beyond the scope of this exploratory paper.

B. Photon spectra

In order to study how much elliptic flow is washed away by other sources of direct photons at RHIC, we need to estimate the other components. We do this by

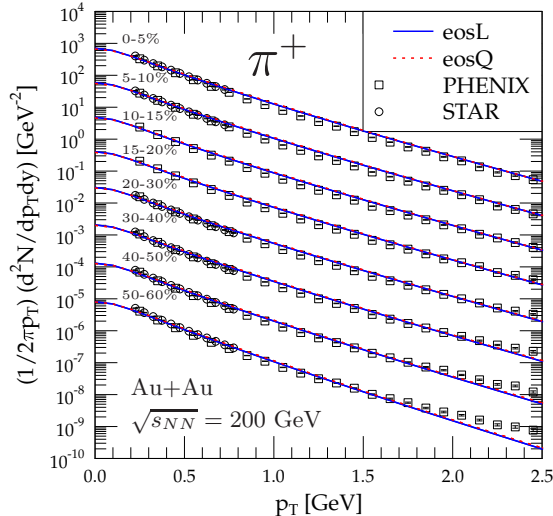


FIG. 3: (Color online) The p_T spectra of positive pions for $\sqrt{s_{NN}} = 200$ GeV Au + Au collisions at RHIC compared with the PHENIX data [42]. The centrality classes are indicated in the figure and the spectra are scaled by increasing powers of 10^{-1} .

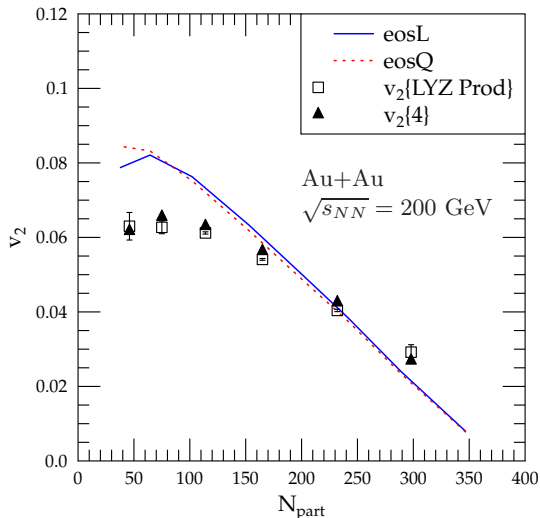


FIG. 4: (Color online) The integrated v_2 for charged hadrons in $\sqrt{s_{NN}} = 200$ GeV Au + Au collisions at RHIC compared with the STAR data [43].

fitting the measured photon p_T spectrum. To study the uncertainties due to the chosen fit functions, we use two different forms. Our first choice ("fit 1") is an exponential combined with a power law function [19]

$$f(p_T) = A \exp(-p_T/T) + \frac{C}{(1 + p_T^2/b)^n}, \quad (10)$$

where A, T, C, b and n are the fit parameters. This fit function is physically motivated by the QCD-like power-law behavior at high p_T and the thermal-like exponential at low p_T . Our alternative choice ("fit 2") is a mere power-law function

$$f(p_T) = \frac{C}{(1 + p_T^2/b)^n}. \quad (11)$$

In these fits, we use the photon data from PHENIX Collaboration. The older data sets [17, 18] have large error bars at low p_T but in the more recent low- p_T data [19] the error bars are much smaller. Unfortunately, the centrality classes in these measurements differ from each other. For our fits shown in Fig. 5, we have simply combined the 0-20% (20-40%) centrality data from Ref. [19] with the 10-20% (30-40%) centrality data from Ref. [18]. In our fits we have included all datapoints from the above sets.

With the fit 1, we first find the parameters b and n by fitting the measured photon p_T spectra in p+p-collisions using the PHENIX data [17, 19] shown in Fig. 5(a). Then for the Au+Au case, keeping the high- p_T slope-parameters b and n fixed, we find A, T and C by fitting the PHENIX data [18, 19] for the two centrality classes shown in Fig. 5. For the fit 2, we use the same data sets. The best fit parameters obtained for the power law fits are listed in Table II and the parameters for the fit 1 can be found in Table III. The fits 1 and 2 have equally small χ^2 values at both centralities.

	Power law fit		
	C [GeV ⁻²]	b [GeV ²]	n
p+p	$3.29 \cdot 10^{-1}$	$4.37 \cdot 10^{-1}$	3.09
Au+Au 0-20%	$2.16 \cdot 10^{14}$	$5.24 \cdot 10^{-5}$	3.35
Au+Au 20-40%	$9.33 \cdot 10^{17}$	$6.35 \cdot 10^{-6}$	3.52

TABLE II: The parameters obtained for the power law fits 2.

	Exponential + power law fit		
	A [GeV ⁻²]	T [GeV]	C
Au+Au 0-20%	85.4	0.212	4.96
Au+Au 20-40%	30.7	0.218	1.18

TABLE III: The parameters for the exponential + power law fits 1. In this case, n and b are obtained from Table II.

In Fig. 5(b) we have replotted the low- and mid- p_T region from Fig. 5(a), and shown our thermal photon results obtained with eosL (eosQ) using the TRG (R92) rates in the HG phase. For clarity, we have plotted the eosL results only for $T_s = 170$ MeV. If we do the switch of the emission rate at $T_s = 200$ MeV, we get 30% (10%) less photons at $p_T = 1(2)$ GeV, because the TRG emission rate is smaller than the QGP emission rate, as shown in Fig. 2.

Our thermal photon results shown in Fig. 5(b) differ by a factor of two at high p_T . Some of this difference comes

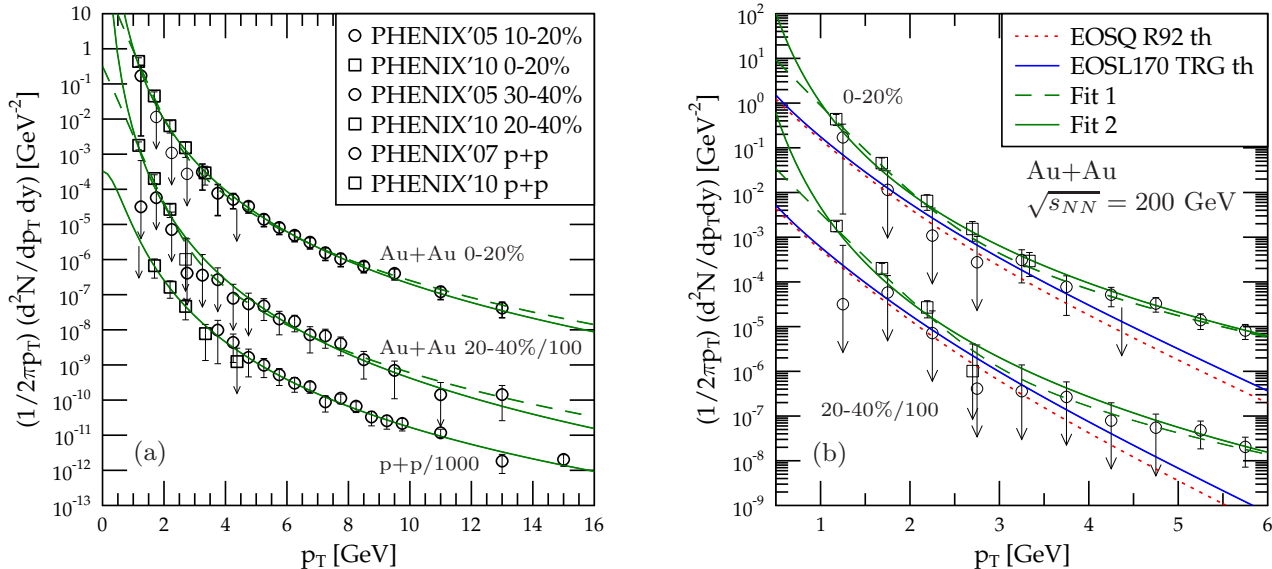


FIG. 5: (Color online) The fits 1 and 2 to the measured photon spectra for two different centralities in $\sqrt{s_{NN}} = 200$ GeV Au+Au collisions and in p+p collisions at $\sqrt{s} = 200$ GeV. The 20-40% centrality-class spectra are divided by 100 and the p+p case by 1000. The data are from the PHENIX Collaboration [17–19]. Our thermal photon results are shown in the panel (b).

from the small difference in the initial temperature profiles which in our case are obtained from the fixed initial entropy density through the EoS. However, a more dominant effect is the different mapping of the energy density to the temperature in eosQ and eosL. The difference in the actual temperature in the two cases is not large but the exponential temperature-dependence in the emission rates magnifies the effect considerably.

From the previous photon studies, see e.g. Refs. [11, 12], we know that photons from HG are contributing mostly at small p_T . In Fig. 5 the difference between the eosQ+R92 and eosL+TRG results shrinks down at low p_T since the R92 HG emission rate is larger than that in the TRG rates and since with eosQ the HG volume becomes larger than with eosL. When we use the TRG rates and eosL, only 3% of the photons come from the HG at $p_T = 1$ GeV. With eosQ and the R92 rates about 50% of the photons originate from HG at the same p_T .

We also note that in the low- p_T region our thermal photon results very clearly undershoot the latest PHENIX data. We have checked that changing the freeze-out temperature to $T_{dec} = 120$ MeV gives only a negligible improvement. This feature is typical to almost all hydrodynamical calculations as can be seen e.g. from Fig. 43 in Ref. [46].

At $p_T \sim 3$ GeV the obtained thermal photon emission is almost enough to match the fit 1 at both centralities if eosL is considered. This suggests that we may have a window for thermal photon dominance at this p_T . However, if we compare with the fit 2 there is always at least a factor of two difference. Event-by-event fluctuations in

the initial state, however, have been shown to increase the thermal emission at $p_T > 2$ GeV [47], and thus we should indeed have a better chance to have a region where the direct photon p_T spectrum, and consequently also the photon v_2 , at RHIC is entirely dominated by the thermal emission.

C. Photon elliptic flow

In Fig. 6(a) we have plotted the elliptic flow of the thermal photons using both eosQ and eosL with the R92 rates. Panel b shows the same calculations but with the TRG rates. Unlike for hadrons, the thermal photon elliptic flow starts to decrease quickly above $p_T \sim 2$ GeV. The reason for this is that practically all high p_T photons are emitted nearly isotropically in the beginning of the evolution (see e.g. Fig. 3 in Ref. [47]), when the hydrodynamical flow effects are very small. Since the photon emission is dominated by the early times the thermal photon elliptic flow is clearly smaller than the hadronic $v_2(p_T)$, which probes the flow anisotropy only on the freeze-out surface.

From Fig. 6(a) we see that the larger switching temperature T_s in eosL only moves the elliptic-flow peak towards higher p_T . However, as shown in Fig. 6(b), with the TRG rates there is factor of two difference in the maximum value between the eosL170 and eosL200 cases. This systematic can be deduced from Fig. 2 and hydrodynamical evolution as follows: When the system reaches the cross-over region near the QCD phase transition, there

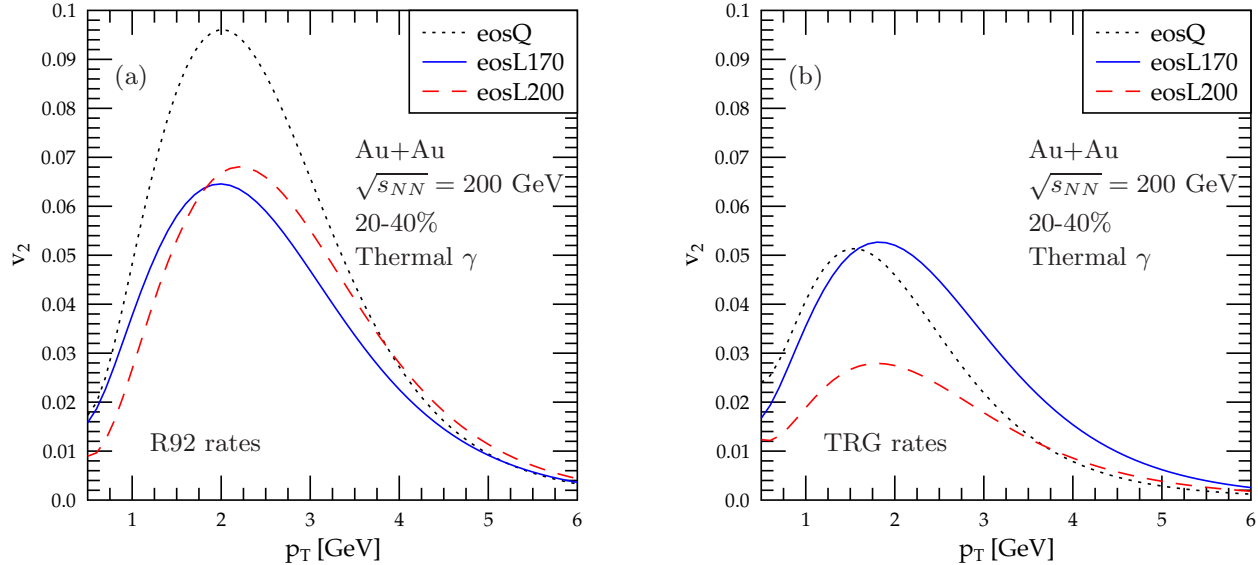


FIG. 6: (Color online) Elliptic flow of thermal photons in Au+Au collisions at $\sqrt{s_{NN}} = 200$ GeV.

has already been a significant anisotropy developed in the transverse flow which is directly reflected to the thermal photon v_2 . Thus, if the photon emission is increased (decreased) in this region, the thermal photon v_2 increases (decreases). As seen in Fig. 2, with the TRG rates the QGP emission rate is larger than the HG rate. Hence increasing the switching temperature decreases the emission and thus the v_2 . This effect is seen in Fig. 6(b). With the R92 rates in Fig. 6(a) the situation is slightly different, as in the cross-over region $T = 170...200$ MeV the QGP emission rate is larger than the HG rate at small energies and vice versa at high energies. Thus, at low- p_T in Fig. 6(a) the situation is similar to panel b (i.e. v_2 is larger for eosL170 than for eosL200). At $p_T > 2$ GeV, the increase of the switching temperature now increases the total emission and thus making v_2 larger for eosL200 than for eosL170.

We also notice from the eosQ results in Fig. 6 that the maximum v_2 decreases by a factor 2 when replacing the R92 rates by the TRG rates. Since the QGP rates in both cases are the same, this signals to us that the hadron gas indeed plays an important role in generating the thermal photon v_2 in the eosQ case. To quantify this statement, we have plotted in Fig. 7 the fraction of photon $v_2(p_T)$ coming from the HG phase. We define v_2^{HG} as

$$v_2^{\text{HG}} = \frac{\int d\phi \cos(2\phi) \frac{dN^{\text{HG}}}{dp_T^2 d\phi dy}}{\int d\phi \frac{dN^{\text{QGP+HG}}}{dp_T^2 d\phi dy}}, \quad (12)$$

i.e. relative to all thermal photons. We see that the photon v_2 can be mostly from the HG (eosQ with R92) or mostly from the QGP (eosL170 with TRG), or between

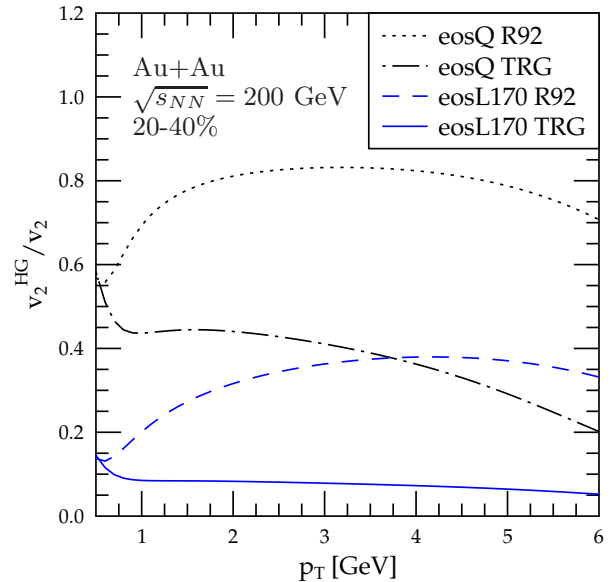


FIG. 7: (Color online) The contribution to the thermal photon elliptic flow from the hadron gas in Au+Au collisions at $\sqrt{s_{NN}} = 200$ GeV.

these extremes (eosQ+TRG and eosL170+R92). Thus, both the EoS and the HG emission rate have a big effect on where the thermal photon v_2 originates from.

Figure 8 illustrates how much elliptic flow of thermal

photons is washed away if we include other direct photon components assuming that they are produced isotropically. We can see that the final photon v_2 , obtained from Eq. (9) based on the fits 1 and 2, is clearly smaller than the thermal one, and also that the different fit functions modify the place and shape of the peak, keeping however the maximum v_2 roughly the same.

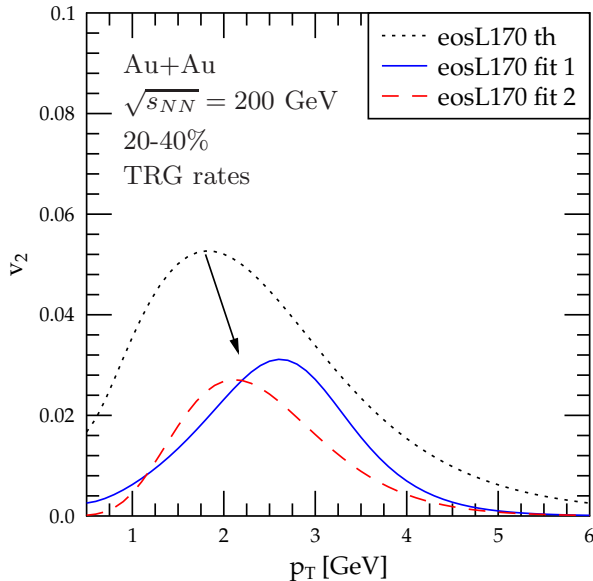


FIG. 8: (Color online) Elliptic flow of thermal and direct photons in Au+Au collisions at $\sqrt{s_{NN}} = 200$ GeV.

Finally, in Fig. 9, we have plotted both the thermal photon and the full direct photon elliptic flow in 0-20% and 20-40% centrality classes for the eosQ+R92 and eosL170+TRG cases. The latter can be considered as a state of the art calculation in that a realistic EoS and latest rates are utilized. In the eosQ+R92 case, the elliptic flow is as large as it can be in our approach. For both cases, the fit 1 is used to estimate how the other components reduce the elliptic flow. As seen in Fig. 5, the thermal photon yield is smaller in the eosQ case, and hence the other direct photon components wash away more of the elliptic flow in the eosQ case than in eosL170 case.

IV. PREDICTION FOR THE LHC

Next, we extrapolate our hydrodynamical modeling to the $\sqrt{s_{NN}} = 2.76$ TeV Pb+Pb collisions at the LHC. We choose the same s_{WN} initial density profile and decoupling temperatures as at RHIC, and, as explained in Sec. II.B, use the measured charged-hadron multiplicity [25] to fix the initial entropy and initial time through the EKRT-model (for details, see Ref. [26]). As

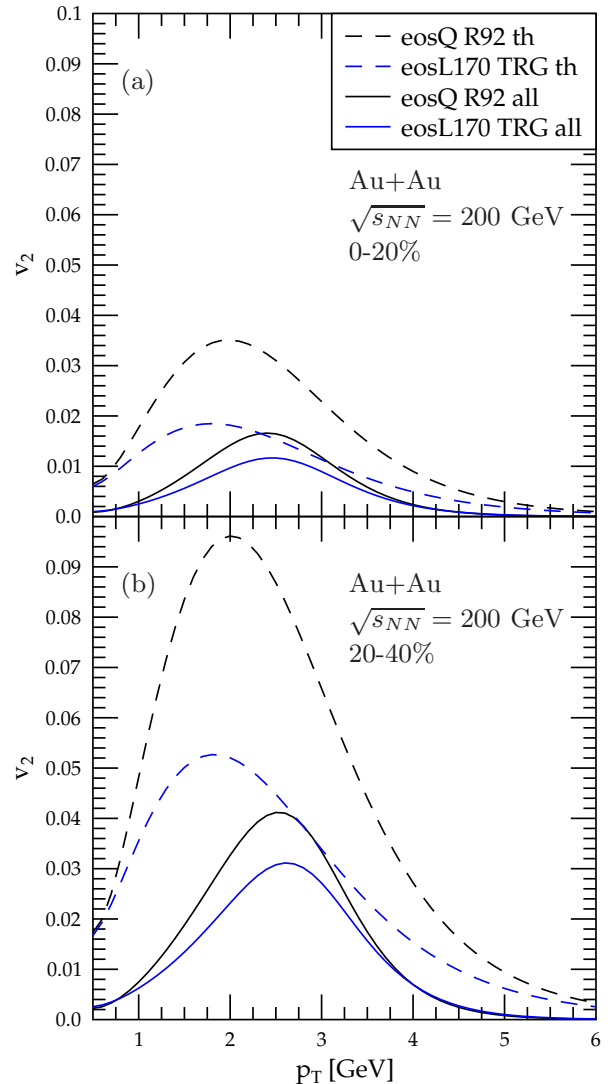


FIG. 9: (Color online) Elliptic flow of direct photons in Au+Au collisions at $\sqrt{s_{NN}} = 200$ GeV.

seen in Fig. 10, a reasonable agreement with the measured charged-hadron p_T spectrum [48] follows up to $p_T \sim 4$ GeV. This ensures that our thermal photon calculations are meaningful also at the LHC energies.

In Fig. 11 we have plotted our prediction for the thermal photon p_T spectrum in the $\sqrt{s_{NN}} = 2.76$ TeV Pb+Pb collisions at the LHC. The bands shown are defined by the cases eosL170+R92 and eosQ+TRG, which give the largest and smallest yields, correspondingly. We see that the uncertainty coming from the EoS and from the HG emission rates is at largest of the order of 40%. We note that these predictions are qualitatively quite similar to the predictions given in [20, 21] for $\sqrt{s_{NN}} = 5.5$ TeV.

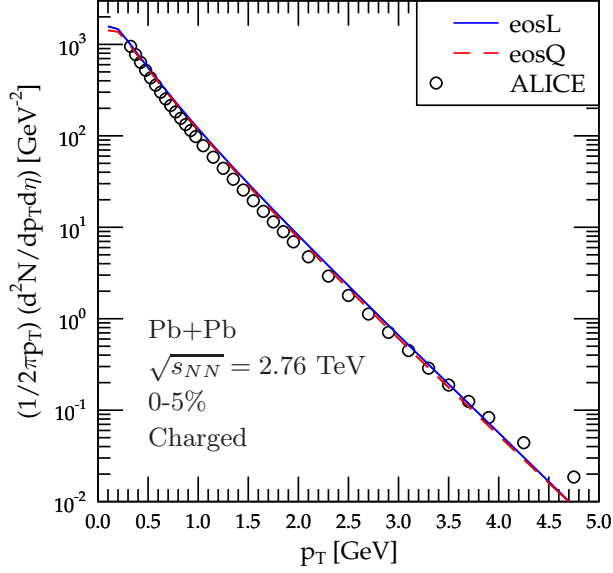


FIG. 10: (Color online) Transverse momentum spectra of charged hadrons in 0-5 % most central Pb+Pb collisions at $\sqrt{s_{NN}} = 2.76$ TeV. Data from ALICE Collaboration [48].

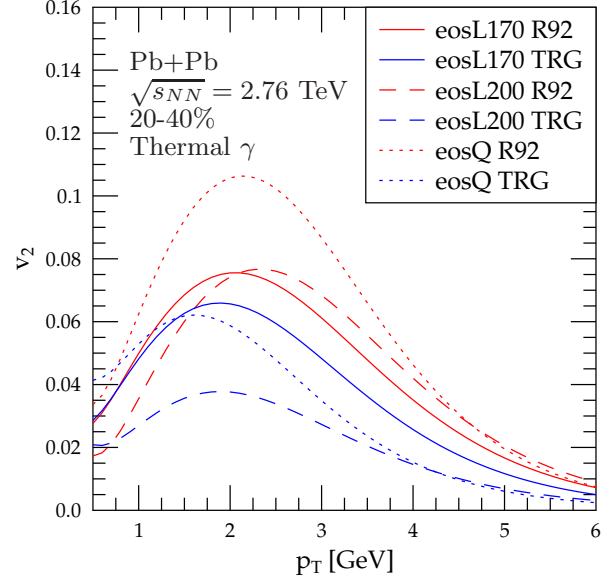


FIG. 12: (Color online) Elliptic flow of thermal photons in Pb+Pb collisions at $\sqrt{s_{NN}} = 2.76$ TeV.

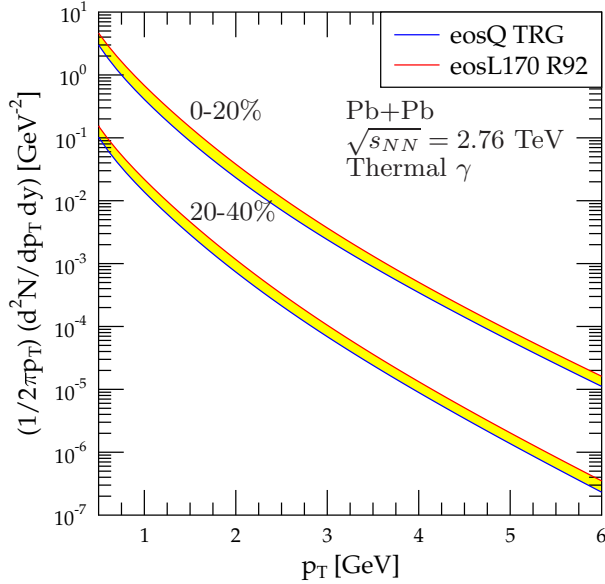


FIG. 11: (Color online) Transverse momentum spectra of thermal photons in Pb+Pb collisions at $\sqrt{s_{NN}} = 2.76$ TeV.

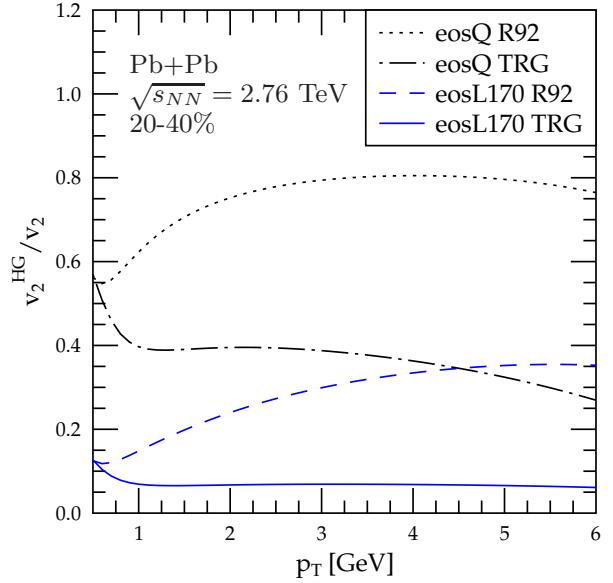


FIG. 13: (Color online) The contribution to the thermal photon elliptic flow from the hadron gas in Pb+Pb collisions at $\sqrt{s_{NN}} = 2.76$ TeV.

Since currently we do not have the measured total direct photon spectrum at the LHC available yet (like we had at RHIC), we can consider only the thermal photon elliptic flow here. It is, however, very interesting to

compare the thermal photon elliptic flow with the RHIC results. We have plotted the obtained thermal photon v_2 in Fig. 12 for 20-40% central collisions. We can see that, similarly to the hadronic case [49], the thermal photon

elliptic flow is very similar at RHIC and LHC. This is a non-trivial result since the temperature-range, flow-range as well as the volume factors for photon emission (from the QGP in particular) are larger at the LHC than at RHIC, and, as discussed in [24] also the flow asymmetry near the phase transition region is larger at the LHC. Then, when going from RHIC to LHC, in order to arrive at a similar v_2 in both cases, the increased flow asymmetry in the numerator of Eq. 6 is compensated by the increased photon yields in the denominator of Eq. 6. In Fig. 13 we again plot the hadronic fraction of $v_2(p_T)$ for the same cases as in Fig. 7. The figure shows that v_2^{HG} is again very close to the corresponding fraction at RHIC.

V. DISCUSSION

We have considered the sensitivity of thermal photon production to the EoS and emission rates in heavy-ion collisions at RHIC and LHC. We have compared the obtained thermal photon yields with the PHENIX measurements, and shown that in the window $2 \lesssim p_T \lesssim 3$ GeV the thermal contribution, computed with a realistic EoS (eosL) and latest emission rates (TRG), is reasonably close to the data. Like in most previous hydrodynamical studies, in the region $p_T \sim 1$ GeV, however, we get a clearly smaller yield than what is measured most recently. We have shown that around $p_T \sim 2$ GeV the thermal photon elliptic flow peaks at a fairly large value, 5 % in the 20-40% centrality class with eosL+TRG, but also that the possible other components may wash even half of this away. We emphasize, however, that the amount of v_2 wash-out depends on the thermal photon contribution relative to the other components. Thermal photon production near $p_T \sim 2$ GeV at RHIC can be expected to in-

crease further once the event-by-event QCD-matter density fluctuations are accounted for [47], in which case the thermal photon production can become dominant and the v_2 wash-out to decrease or even vanish.

Constraining our hydrodynamical modeling with the measured charged-hadron spectrum in $\sqrt{s_{NN}} = 2.76$ TeV Pb+Pb collisions at the LHC, we have predicted the thermal photon p_T spectra and v_2 . According to our results, elliptic flow of thermal photons at the LHC and RHIC are very similar in the few- p_T region. For the determination of a possible thermal photon window, and consequently thermal photon v_2 , it will be extremely interesting to see the direct photon data at the LHC.

Next, one should consider the effects of event-by-event density fluctuations [44, 50–54] on thermal photon elliptic flow. On the theoretical side, one would need a better understanding of how the degrees of freedom in the QGP would be best accounted for when computing thermal photon production, as well as a better control over the photon emission in the phase transition region. Also the dissipative hydrodynamical effects to thermal photon production should be studied further, so far only the very first steps into this direction have been taken, see Ref. [55].

Acknowledgments

We gratefully acknowledge financial support by the Academy of Finland, KJE's project 133005. In addition, HH is supported by the national Graduate School of Particle and Nuclear Physics. We acknowledge CSC – IT Center for Science in Espoo, Finland, for the allocation of computational resources. We would like to thank R. Chatterjee for useful discussions.

-
- [1] S. S. Adler *et al.* [PHENIX Collaboration], Phys. Rev. Lett. **96** (2006) 202301.
 - [2] P. Aurenche, M. Fontannaz, J. -P. Guillet, E. Pilon, M. Werlen, Phys. Rev. **D73** (2006) 094007.
 - [3] F. Arleo, K. J. Eskola, H. Paukkunen, C. A. Salgado, JHEP **1104** (2011) 055.
 - [4] K. J. Eskola, H. Paukkunen, C. A. Salgado, JHEP **0904** (2009) 065.
 - [5] R. J. Fries, B. Muller, D. K. Srivastava, Phys. Rev. Lett. **90** (2003) 132301.
 - [6] R. J. Fries, B. Muller, D. K. Srivastava, Phys. Rev. **C72** (2005) 041902.
 - [7] S. Turbide, C. Gale, E. Frodermann, U. Heinz, Phys. Rev. **C77** (2008) 024909.
 - [8] F. -M. Liu, T. Hirano, K. Werner, Y. Zhu, Phys. Rev. **C79** (2009) 014905.
 - [9] G. -Y. Qin, J. Ruppert, C. Gale, S. Jeon, G. D. Moore, Phys. Rev. **C80** (2009) 054909.
 - [10] P. Huovinen, P. V. Ruuskanen, J. Sollfrank, Nucl. Phys. **A650** (1999) 227-244.
 - [11] P. Huovinen, P. V. Ruuskanen, S. S. Räsänen, Phys. Lett. **B535** (2002) 109-116.
 - [12] S. S. Räsänen, Nucl. Phys. **A715** (2003) 717-725.
 - [13] D. G. d'Enterria, D. Peressounko, Eur. Phys. J. **C46** (2006) 451-464.
 - [14] R. Chatterjee, E. S. Frodermann, U. W. Heinz, D. K. Srivastava, Phys. Rev. Lett. **96** (2006) 202302.
 - [15] R. Chatterjee, D. K. Srivastava, Phys. Rev. **C79** (2009) 021901.
 - [16] F. -M. Liu, T. Hirano, K. Werner, Y. Zhu, Phys. Rev. **C80** (2009) 034905.
 - [17] S. S. Adler *et al.* [PHENIX Collaboration], Phys. Rev. Lett. **98** (2007) 012002.
 - [18] S. S. Adler *et al.* [PHENIX Collaboration], Phys. Rev. Lett. **94** (2005) 232301.
 - [19] A. Adare *et al.* [PHENIX Collaboration], Phys. Rev. Lett. **104** (2010) 132301.
 - [20] F. Arleo *et al.*, *Photon Physics in Heavy Ion Collisions*, CERN Yellow Book report (2004), hep-ph/0311131.
 - [21] K. Dusling, I. Zahed, Phys. Rev. **C82** (2010) 054909.
 - [22] K. J. Eskola, K. Kajantie, P. V. Ruuskanen, K. Tuominen, Nucl. Phys. **B570** (2000) 379-389.

- [23] K. J. Eskola, H. Honkanen, H. Niemi, P. V. Ruuskanen, S. S. Rasanen, Phys. Rev. **C72** (2005) 044904.
- [24] H. Niemi, K. J. Eskola, P. V. Ruuskanen, Phys. Rev. **C79** (2009) 024903.
- [25] K. Aamodt *et al.* [The ALICE Collaboration], Phys. Rev. Lett. **105** (2010) 252301.
- [26] T. Renk, H. Holopainen, R. Paatelainen, K. J. Eskola, arXiv:1103.5308 [hep-ph].
- [27] B. I. Abelev *et al.* [STAR Collaboration], Phys. Rev. **C79** (2009) 034909.
- [28] P. F. Kolb, U. W. Heinz, P. Huovinen, K. J. Eskola, K. Tuominen, Nucl. Phys. **A696** (2001) 197-215.
- [29] J. P. Boris, D. L. Book, J. Comput. Phys. **A11** (1973) 38.
- [30] S. T. Zalesak, J. Comput. Phys. **A31** (1979) 248.
- [31] J. Sollfrank, P. Huovinen, M. Kataja, P. V. Ruuskanen, M. Prakash, R. Venugopalan, Phys. Rev. C **55** (1997) 392.
- [32] M. Laine, Y. Schroder, Phys. Rev. **D73** (2006) 085009.
- [33] P. Huovinen, P. Petreczky, Nucl. Phys. **A837** (2010) 26-53.
- [34] F. Cooper, G. Frye, Phys. Rev. **D10** (1974) 186.
- [35] P. B. Arnold, G. D. Moore, L. G. Yaffe, JHEP **0111** (2001) 057.
- [36] P. B. Arnold, G. D. Moore, L. G. Yaffe, JHEP **0112** (2001) 009.
- [37] F. Karsch, Z. Phys. **C38** (1988) 147.
- [38] J. I. Kapusta, P. Lichard, D. Seibert, Phys. Rev. **D44** (1991) 2774.
- [39] L. Xiong, E. V. Shuryak, G. E. Brown, Phys. Rev. **D46** (1992) 3798-3801.
- [40] H. Nadeau, J. I. Kapusta, P. Lichard, Phys. Rev. **C45** (1992) 3034.
- [41] S. Turbide, R. Rapp, C. Gale, Phys. Rev. **C69** (2004) 014903.
- [42] S. S. Adler *et al.* [PHENIX Collaboration], Phys. Rev. **C69** (2004) 034909.
- [43] B. I. Abelev *et al.* [STAR Collaboration], Phys. Rev. **C77** (2008) 054901.
- [44] H. Holopainen, H. Niemi, K. J. Eskola, Phys. Rev. **C83** (2011) 034901.
- [45] P. Romatschke, U. Romatschke, Phys. Rev. Lett. **99** (2007) 172301.
- [46] A. Adare *et al.* [PHENIX Collaboration], Phys. Rev. **C81** (2010) 034911.
- [47] R. Chatterjee, H. Holopainen, T. Renk, K. J. Eskola, arXiv:1102.4706 [hep-ph].
- [48] K. Aamodt *et al.* [ALICE Collaboration], Phys. Lett. **B696** (2011) 30-39.
- [49] K. Aamodt *et al.* [The ALICE Collaboration], arXiv:1011.3914 [nucl-ex].
- [50] R. P. G. Andrade, F. Grassi, Y. Hama, T. Kodama, W. L. Qian, Phys. Rev. Lett. **101** (2008) 112301.
- [51] H. Petersen, M. Bleicher, Phys. Rev. **C81** (2010) 044906.
- [52] K. Werner, I. Karpenko, T. Pierog, M. Bleicher, K. Mikhailov, Phys. Rev. **C82** (2010) 044904.
- [53] B. Schenke, S. Jeon, C. Gale, Phys. Rev. Lett. **106** (2011) 042301.
- [54] Z. Qiu, U. W. Heinz, arXiv:1104.0650 [nucl-th].
- [55] K. Dusling, Nucl. Phys. **A839** (2010) 70-77.